

HIGHLIGHTED ARTICLE

Frontline Science: Employing enzymatic treatment options for management of ocular biofilm-based infections

Abirami Kugadas¹ | Jennifer Geddes-McAlister² | Emilia Guy¹ |
 Antonio DiGiandomenico³ | David B. Sykes⁴ | Michael K. Mansour⁵ |
 Rossen Mirchev⁶ | Mihaela Gadjeva¹

¹Department of Medicine, Division of Infectious Diseases, Brigham and Women's Hospital, Harvard Medical School, Boston, Massachusetts, USA

²Proteomics and Signal Transduction Department, Max Planck Institute of Biochemistry, Martinsried, Germany

³MedImmune, LLC, Gaithersburg, Maryland, USA

⁴Center for Regenerative Medicine, Massachusetts General Hospital, Boston, Massachusetts, USA

⁵Division of Infectious Diseases, Massachusetts General Hospital, Boston, Massachusetts, USA

⁶Biological Chemistry and Molecular Pharmacology, Harvard Medical School, Boston, Massachusetts, USA

Correspondence

Mihaela Gadjeva, Division of Infectious Disease, Brigham and Women's Hospital, 181 Longwood Ave., Boston, MA 02115, USA.
 Email: mgadjeva@rics.bwh.harvard.edu

Abstract

Pseudomonas aeruginosa-induced corneal keratitis is a sight-threatening disease. The rise of antibiotic resistance among *P. aeruginosa* keratitis isolates makes treatment of this disease challenging, emphasizing the need for alternative therapeutic modalities. By comparing the responses to *P. aeruginosa* infection between an outbred mouse strain (Swiss Webster, SW) and a susceptible mouse strain (C57BL6/N), we found that the inherent neutrophil-killing abilities of these strains correlated with their susceptibility to infection. Namely, SW-derived neutrophils were significantly more efficient at killing *P. aeruginosa* in vitro than C57BL6/N-derived neutrophils. To interrogate whether the distinct neutrophil killing capacities were dependent on endogenous or exogenous factors, neutrophil progenitor cell lines were generated. The in vitro differentiated neutrophils from either SW or C57BL6/N progenitors retained the differential killing abilities, illustrating that endogenous factors conferred resistance. Consistently, quantitative LC-MS/MS analysis revealed strain-specific and infection-induced alterations of neutrophil proteomes. Among the distinctly elevated proteins in the SW-derived proteomes were α -mannosidases, potentially associated with protection. Inhibition of α -mannosidases reduced neutrophil bactericidal functions in vitro. Conversely, topical application of α -mannosidases reduced bacterial biofilms and burden of infected corneas. Cumulatively, these data suggest novel therapeutic approaches to control bacterial biofilm assembly and improve bacterial clearance via enzymatic treatments.

KEYWORDS

biofilms, innate immunity, neutrophils, *P. aeruginosa*

1 | INTRODUCTION

Eye trauma and contact lens use are the main factors that predispose to the development of infectious keratitis associated with vision loss and blindness.^{1,2} In the United States, 1 in 2500 daily contact wearers and 1 in 500 overnight lens wearers develop bacterial keratitis, which constitutes a significant health problem. The organism that is most often isolated from contact lens-associated corneal ulcers is *Pseudomonas aeruginosa*.^{3,4} Existing therapies often fail to eradicate *P. aeruginosa* efficiently due to pathoadaptation and acquired antibiotic resistance, marking the need to find alternative

therapeutic approaches.⁵ Therefore, there is a significant interest in developing strategies to strengthen host resistance to infection.

The effective control and clearance of *P. aeruginosa* depends on engulfment, phagocytosis, and degradation of bacteria in a complex and highly regulated process that works in concert with other innate immune responses, such as inflammatory signals. Genetic deficiencies that compromise phagocytosis, reactive oxygen species (ROS) production, and phagocyte trafficking and adhesion result in a significant predisposition to infection.⁶ In addition, bacteria harbor versatile mechanisms to reduce phagocyte functionality. For example, *P. aeruginosa* alters the dynamics of cytoskeletal changes associated with

Abbreviations: CHO, chinese hamster ovary; GCSF, granulocyte colony stimulating factor; PMN, polymorphonuclear cells

This is an open access article under the terms of the Creative Commons Attribution-NonCommercial-NoDerivs License, which permits use and distribution in any medium, provided the original work is properly cited, the use is non-commercial and no modifications or adaptations are made.

©2019 The Authors. *Society for Leukocyte Biology* Published by Wiley Periodicals, Inc.

Received: 24 September 2018 | Revised: 15 January 2019 | Accepted: 16 January 2019

J Leukoc Biol. 2019;105:1099–1110.

www.jleukbio.org | 1099

phagocytosis, blocks ROS synthesis, and escapes phagocytic vacuoles via effectors released by the type III secretion system.^{7–10}

Although *P. aeruginosa* can proliferate in the cytosol of phagocytic cells,^{11,12} the majority of it is present extracellularly. During chronic infection, *P. aeruginosa* forms biofilms at mucosal sites, where it resides in a nonmotile and protected from phagocytosis state. In biofilms, bacteria increase the synthesis of extracellular polysaccharides (EPS) to generate biomatrix in which the individual bacterial cells are embedded. Three different types of polysaccharides—Psl, Pel, and alginate—have been described as essential to biofilm formation.^{13–20} Importantly, the different polysaccharides demonstrate distinct production kinetics, suggesting differential impact on the biofilm growth.²¹ Whether *P. aeruginosa* forms biofilms during acute infections such as ocular keratitis remains controversial.²²

Interestingly, in biofilms *P. aeruginosa* is surrounded by neutrophils, which fail to breach bacterial structures resulting in a limited host response.²³ It is proposed that the EPS matrix that covers *P. aeruginosa* biofilms inhibits complement activation and neutrophil phagocytosis^{24,25} due to entrapped active enzymes, such as ecotin, a Psl-binding protein with serine protease inhibitory that may inhibit complement convertase activation. Here, we describe a mechanism of biofilm decomposition activated in neutrophils derived from a strain of mice resistant to keratitis. We show that the production of polysaccharide degrading enzymes, including α -mannosidases, is elevated leading to more efficient biofilm breakdown. We propose that the production of enzymes that solubilize biofilms is a novel mechanism for anti-bacterial protection. Our work suggests that these enzymes could harbor therapeutic potential for treatment of infectious diseases.

2 | MATERIALS AND METHODS

2.1 | Ethics statement

All animal experiments were performed following National Institutes of Health guidelines for housing and care of laboratory animals and performed in accordance with institutional regulations after protocol review and approval by BWH IACUC committee and were consistent with the Association for Research in Vision and Ophthalmology guidelines for studies in animals (protocol 311).

2.2 | Mice

Mice were housed and bred at the MCP Animal Care Facility. Swiss Webster (SW) and C57BL/6N mice were purchased from Taconic Farms (Rensselaer, NY). Seven- to 9-wk-old mice were used throughout the experiments. We have not observed significant differences in the bacterial clearance of male and female mice to ocular *P. aeruginosa*-induced infection.

2.3 | Bacterial strains and inocula

Invasive *P. aeruginosa* clinical isolate 6294-GFP and PAO1-GFP strain were used throughout the experiments. For the imaging experiments, *P. aeruginosa* strains and clinical isolates PAO1, and 6354 were electro-

porated with pCdrA-GFP (kindly provided by Prof. Tolker-Nielsen²⁶) and selected on gentamicin (15 μ g/ml). The bacterial strains were grown overnight at 37°C on Tryptic Soy Broth (TSB) (Cardinal Health, Dublin, OH) agar plates supplemented with 5% sheep blood. Bacterial suspensions were prepared in saline solution and used for subsequent infection experiments.

2.4 | Infection model

Infections were carried out as described previously.²⁷ Briefly, mice were anesthetized with intraperitoneal ketamine and xylazine injections. Three 5 mm scratches were made on the cornea with 25G needle tip and an inoculum of 1×10^5 CFU of *P. aeruginosa* was delivered in 5 μ l onto the eye. Mice remained sedated for approximately 30 min. For evaluation of corneal pathology, daily scores were recorded by an observer unaware of the experimental conditions based on the following scoring system using a graded scale of 0 to 4 as follows: 0, eye macroscopically identical to the uninfected contra-lateral control eye; 1, faint opacity partially covering the pupil; 2, dense opacity covering the pupil; 3, dense opacity covering the entire anterior segment; and 4, perforation of the cornea, phthisis bulbi (shrinkage of the globe after inflammatory disease), or both. To determine corneal bacterial counts at 24 h after infection, mice were sacrificed, the eyes were enucleated, and the corneas were dissected from the ocular surface. To quantify *P. aeruginosa* levels, corneas were suspended in PBS, 0.05% Triton X100, serially diluted and plated on *P. aeruginosa* selective McConkey agar plates.

2.5 | Purification of Polymorphonuclear cells (PMNs) and bactericidal assays

Murine bone marrow was flushed from both hind limbs with PBS supplemented with 2% FBS and 1 mM EDTA. The cells were washed, erythrocytes in the cell pellet were lysed using the Mouse Erythrolysis Kit (R&D Systems, Minneapolis, MN) according to the manufacturer's instruction, and neutrophils were isolated using the EasySep Mouse Neutrophil Enrichment Kit (Vancouver, Canada). Neutrophils were incubated with *P. aeruginosa* strain PAO1 at an MOI of 100:1 for 90 min at 37°C on a rotator. Aliquots taken at time 0 and 90 min were serially diluted and plated on McConkey agar to determine numbers of live *P. aeruginosa*. Percentage of killing ability of neutrophils was calculated.²⁸

2.6 | Neutrophil cell lines and treatments

SW and C57BL6/N neutrophil progenitor cell lines were established as described in.²⁹ Neutrophil progenitors were maintained in RPMI supplemented with 10% FBS, penicillin-streptomycin, stem cell factor (SCF), and β -estradiol. The SCF was supplied as conditioned media from a Chinese Hamster Ovary cell line engineered to produce SCF. A total of 2% conditioned media was used, equating to a SCF concentration of ~ 100 ng/ml. The β -estradiol (Sigma, Ronkonkoma, NY, USA) was dissolved in ethanol at 10 mM stock and used at a final concentration of 0.5 μ M. To differentiate into granulocytes, β -estradiol was omitted from the growth media, and cells were cultured in RPMI media

supplemented with 20 ng/ml granulocyte colony stimulating factor (GCSF) (BioLegend, San Diego, CA, USA), 10% FBS, penicillin-streptomycin, and maintained for either 3 or 5 days before performing the killing experiments. Typically, 1.5×10^6 granulocytes were either treated with swainsonine (Tocris, Minneapolis, MN, USA) at a final concentration of 1 $\mu\text{g}/\text{ml}$ or vehicle control for 2–3 h at 37°C 5% CO_2 before adding or murine serum and *P. aeruginosa* 6294. The bactericidal assay was performed as described above.

2.7 | Intravital imaging

To image EPS, fluorescently labelled 0.5 μg mAb to Psl Cam003,³⁰ alginate F429¹⁹ or control human IgG1¹⁹ were topically applied to the cornea for 15 min, ocular surface was washed thrice with 15 μl of PBS before imaging. To visualize neutrophils, C57BL6/N mice were injected with 5 μg fluorescently labelled anti-Ly6G (with either Alexa 674 or APC) (Thermo Fisher Scientific, Bremen, Germany) IV for 30 min to 1 h before imaging.³¹ Video was acquired with an upright Olympus FV1000 intravital microscope (Center Valley, PA, USA). The microscope was equipped with a LumPlan 40 \times /0.8 numerical aperture (NA) 20 \times water immersion objective and digitally recorded with an Olympus DP71 charge-coupled device video camera and Olympus FluoView 1000 imaging software. Some experiments were carried out using the imaging system as described in.⁸ Images and 3D reconstructions were carried out using Image J and MatLab. Areas covered with bacterial biofilms were calculated and compared across different time points of biofilm growth. Neutrophil meandering index was calculated per individual tracks derived from at least 30 individual neutrophils per separate imaging. Meandering index was calculated as a ratio of displacement per individual track length.

2.8 | Sample preparation for LC-MS/MS analysis

PMNs from infected and baseline SW and C57BL6/N mice (in triplicate or quadruplicate) were subjected to in-solution trypsin digestion. Briefly, 200 μl of 8 M Urea containing 40 mM HEPES was added to baseline and infected SW and C57BL6/N samples were sonicated in a rotating water bath at 4°C for 15 min (30 s on, 30 s off). The samples were then reduced with 10 mM DTT, alkylated with 55 mM iodoacetamide (IAA), followed by dilution with 50 mM ammonium bicarbonate to 2 M urea, and LysC and trypsin (protein: enzyme ratio 50:1) digestion overnight. Digestion was stopped by addition of 10% v/v trifluoroacetic acid (TFA) per sample and the acidified peptides were loaded onto StageTips (containing three layers of C_{18}) to desalt and purify according to the standard protocol.³² Each sample was divided onto two StageTips (one “working” and one “back-up”) and stored at 4°C until the LC-MS/MS measurement.

2.9 | LC MS/MS measurement

Samples were eluted from StageTips with 50 μl buffer B (80% acetonitrile [ACN] and 0.5% acetic acid), the organic solvent was removed in a SpeedVac concentrator for 20 min, and peptides were resuspended in 10 μl of buffer A (2% ACN and 0.1% TFA). 3 μl of each sample was analyzed by nanoflow liquid chromatography on an EASY-nLC system

(Thermo Fisher Scientific) online coupled to an Q Exactive HF-X quadrupole orbitrap mass spectrometer (Thermo Fisher Scientific) through a nanoelectrospray ion source (Thermo Fisher Scientific). A 50 cm column with 75 μm inner diameter was used for the chromatography, in-house packed with 3 μm reversed-phase silica beads (ReproSil-Pur C_{18} -AQ, Dr. Maisch, GmbH, Ammerbuch, Germany). Peptides were separated and directly electrosprayed into the mass spectrometer using a linear gradient from 5% to 60% ACN in 0.5% acetic acid over 120 min at a constant flow of 300 nl/min. The linear gradient was followed by a washout with up to 95% ACN to clean the column for the next run. The overall gradient length was 145 min. The QExactive HF-X was operated in a data-dependent mode, switching automatically between one full scan and subsequent MS/MS scans of the fifteen most abundant peaks (Top15 method), with full scans (m/z 300–1650) acquired in the Orbitrap analyzer with a resolution of 60,000 at 100 m/z .

2.10 | Raw data processing

Raw files were analyzed together using MaxQuant software (version 1.5.6.2).³³ The derived peak list was searched with the built-in Andromeda search engine^{34,35} against the reference *Mus musculus* proteome downloaded from Uniprot (<http://www.uniprot.org/>) (April 27, 2016; 53,106 sequences). The parameters were as follows: strict trypsin specificity was required with cleavage at the C-terminal after K or R, allowing for up to two missed cleavages. The minimum required peptide length was set to seven amino acids. Carbamidomethylation of cysteine was set as a fixed modification (57.021464 Da) and N-acetylation of proteins N termini (42.010565 Da) and oxidation of methionine (15.994915 Da) were set as variable modifications. PSM and protein identifications were filtered using a target-decoy approach at a false discovery rate (FDR) of 1%. ‘Match between runs’ was enabled with a match time window of 0.7 min and an alignment time window of 20 min. Relative, label-free quantification of proteins was done using the MaxLFQ algorithm³⁵ integrated into MaxQuant using a minimum ratio count of 2, enabled FastLFQ option, LFQ minimum number of neighbors at 3, and the LFQ average number of neighbors at 6. The mass spectrometry proteomics data have been deposited in the PRIDE partner repository for the ProteomeXchange Consortium with the data set identifier: PXD009767.

2.11 | Data analysis

Further analysis of the MaxQuant-processed data was performed using the Perseus software environment (version 1.5.5.5).³⁶ The “proteingroups.txt” file was loaded into Perseus. Hits to the reverse database, contaminants, and proteins only identified with modified peptides were eliminated. LFQ intensities were converted to a log scale (\log_2), and only those proteins which were present in triplicate within at least one sample set were used for further statistical analysis (valid-value filter of 3 in at least one group). Missing values were imputed from a normal distribution (downshift of 1.8 standard deviations and a width of 0.3 standard deviations). The total matrix was imputed using these values, enabling statistical analysis. A Welch’s t test was performed to identify proteins with a significant differential

expression (P value < 0.05) between baseline and infected SW and C57BL6/N ($SO = 1$) samples employing a 5% permutation-based FDR filter. A principle component analysis (PCA) was performed to determine proteome differences at the experiment level, as well as Pearson correlation with hierarchical clustering by Euclidean distance to determine replicate reproducibility. A two-sample Student's t test ($SO = 1$) was performed on the entire data set and a 1D-annotation enrichment based on the t test differences with a Benjamini-Hochberg FDR cutoff at 0.05 allowed for visualization of enrichment by keywords within the RStudio platform (<http://www.R-project.org/>). Specifically, annotation enrichment categories meeting the P value (0.05) and FDR (0.05) cutoffs, along with scores < -0.5 and < 0.5 were plotted.

2.12 | In vitro biofilm assays

Single colony of *P. aeruginosa* 6294 was transferred to 3 ml of LB media and grown overnight to $OD_{650} = 1.9$ to 2.1. The overnight culture was diluted to $OD_{650} = 0.5$ with M63 media and seeded into 96-well plates for either 12 h at 37°C. Wells were emptied, washed with PBS, and 125 μ l of 0.5% crystal violet solution added into each well. After 15 min incubation, plates were washed 3 times by submerging into distilled water and blotting vigorously on paper towel. Plates were dried overnight and 125 μ l of 30% acetic acid added into each well to solubilize the crystal. Biofilms were quantified at 600 nm.

2.13 | Mannosidase treatments

C57BL6/N mice were infected with 5×10^5 CFU of *P. aeruginosa* 6294 delivered in 5 μ l onto the eye as described above. Alpha-mannosidase (New England Biolabs, Ipswich, MA, USA) (0.2 U/cornea) were applied topically every 3 h after the infectious challenge for the duration of 12 h. Mice were rested for 12 h and infected corneas harvested at 24 h postinfectious challenge. The control group received topical aliquots of mannosidase buffer.

2.14 | Monoclonal antibody treatments

C57BL6/N mice were infected as described above with *P. aeruginosa* 6294 delivered in 5 μ l onto the eye as described above. A total of 400 μ g of anti-Psl mAb Cam 003 [30] or isotype control Ab were applied topically every 6 h after the infectious challenge for the duration of 24 h.

2.15 | Statistical analysis

Statistical analysis of corneal pathology scores, bacterial burden, and cytokine levels were either by unpaired Student's t test upon normal distribution, Mann-Whitney U test for pairwise comparisons, or one-way ANOVA with Dunn's correction for multigroup comparisons (Prism 4.0 for Macintosh). The analysis of the data from the bactericidal activity assays was based on the use of unpaired Student's t test or One-way ANOVA as appropriate. Differences were considered significant if the P value was < 0.05 (Prism 4.0 for Macintosh).

3 | RESULTS

3.1 | Neutrophils fail to penetrate Psl-containing *P. aeruginosa* biofilms at ocular surfaces

Biofilms are defined as clusters of bacteria encapsulated in EPS. Intravital detection of biofilms during keratitis has been challenging because of a lack of EPS-specific reagents. Recent investigation based on cryo-electron microscopy imaging showed that *P. aeruginosa* formed bacterial microclusters on ocular surfaces, consistent with biofilm formation, but the nature of the EPS was not explored.²² Using intravital imaging, we monitored *P. aeruginosa* PAO1 expressing CdrA-driven GFP behavior during infection.²⁶ This was combined with analysis of the EPS composition by use of fluorescently labelled anti-Psl mAb Cam 003 that specifically recognizes Psl.³⁰ During the early stages of infection, bacteria formed individual bacterial clusters or microcolonies likely emanating from infected epithelial cells (early biofilms) (Fig. 1A), whereas at later time points biofilms were observed where bacteria resided in sheets (late biofilms) (Fig. 1A). Expectedly, bacterial biofilms grew in size during infection (Fig. 1A). The biofilms were surrounded with Psl (Fig. 1C). In contrast to Psl, low abundance of alginate presence was detected (data not shown) and the alginate-deficient clinical *P. aeruginosa* isolate 6354 formed biofilms at ocular surfaces (data not shown), indicative that alginate presence was not required for ocular biofilm formation. Cumulatively, these data suggest that Psl is a dominant polysaccharide among the ones tested making it a rational target for treatment.

We utilized intravital imaging to directly monitor *P. aeruginosa* behavior during ocular infection (Figs. 2 and S1) and found that bacterial biofilms were protected from neutrophil infiltration (Figs. 2, S1, and S2). PMNs approached bacterial biofilms in swarms (Figs. 2A, top right corner and S1). Individual PMNs were visible at the border of the biofilms (Fig. 2A, yellow line) where they showed decreased motilities when compared to the motilities of neutrophils within the swarm or at sites where planktonic bacteria were visible (S1). Neutrophils probed biofilms by extending phyllopodia against bacterial biofilms, but could not easily penetrate biofilms (S2). These data suggest that intervention strategies to disrupt biofilms could improve neutrophil function by permitting access to bacteria themselves.

3.2 | mAbs against Psl improves opsonophagocytosis in vitro but shows no therapeutic efficacy in vivo

The use of Psl-specific mAbs was previously reported to demonstrate good prophylactic efficacy in a lung and keratitis infection models after systemic administration.³⁰ Here, we evaluated the opsonophagocytic killing (OPK) activity of anti-Psl mAb Cam003 against keratitis isolates, examined its bactericidal efficacy against *P. aeruginosa* grown in a planktonic and micro-aggregated forms, and its therapeutic ability in vivo. Consistent with previous data the anti-Psl mAb Cam003 showed significant OPK activity against keratitis clinical *P. aeruginosa* isolates 6294, 6354, and laboratory strain PAO1 (data not shown).³⁰ Notably, the OPK activity was diminished when *P. aeruginosa* was grown in the presence of eukaryotic cells to allow micro-aggregate formation

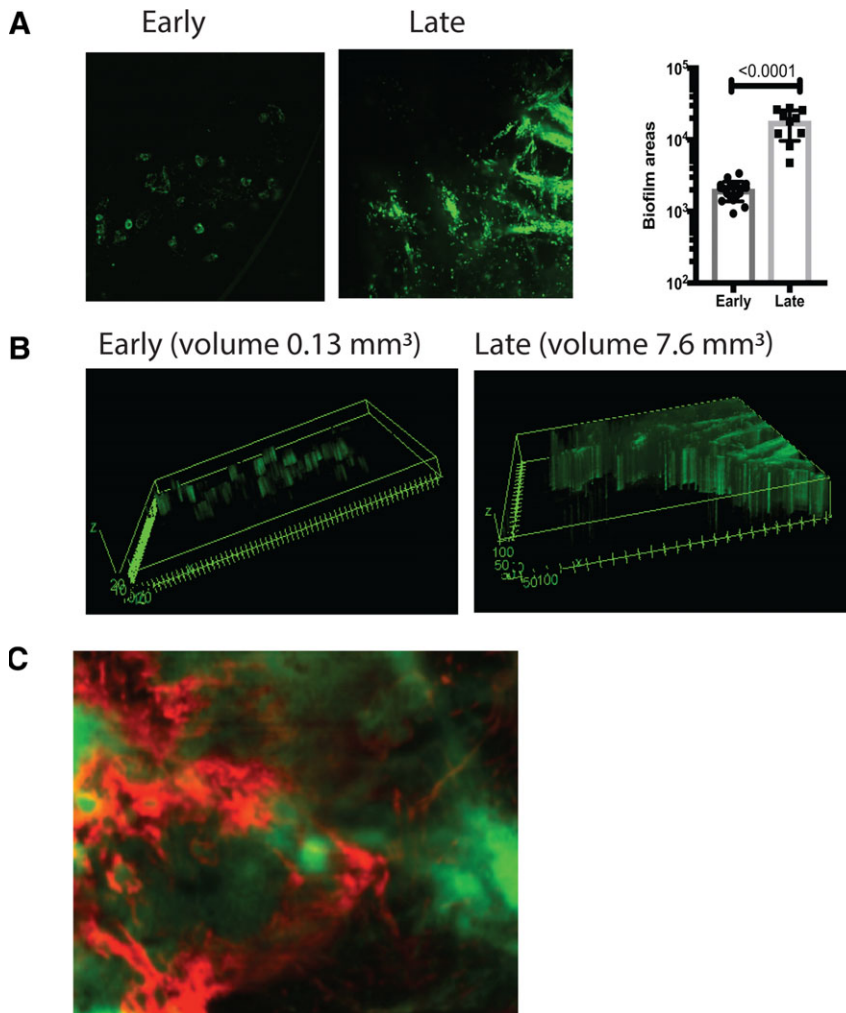


FIGURE 1 *P. aeruginosa* biofilms are surrounded by *psl*. (A) C57BL6/N mice were infected with 1.10^5 CFU/eye *P. aeruginosa* PAO1 expressing CrdA-GFP. The intravital microscopy was carried out at early (12 h) and late (24 h) postinfectious challenge. Individual mice were imaged longitudinally. Areas covered with bacterial microcolonies or biofilms were calculated using Image J analysis. Each symbol represents individual bacterial cluster/microcolony. Student's *t* test. (B) 3D-reconstructions of early and late bacterial biofilms. Volumes of biofilms per image were shown for comparison. (C) Biofilms were stained with fluorescently labeled anti-Psl mAb Cam003 (red), which was applied topically 15 min before imaging. Images were recorded at 40 \times . Psl (red) staining was adjacent or co-localized to *P. aeruginosa* (green). All images are representative of five individual experiments with 1–2 imaged mice per experiment. Imaging across central cornea revealed that bacterial microaggregates were seen during early hours of infection, whereas bacterial biofilms were formed as infection progressed. *P. aeruginosa* PAO1 CdrA-GFP (green) clusters were surrounded by red Psl-stained polysaccharide, consistent with the definition of a biofilm

(Fig. 3A). However, despite these prominent *in vitro* effects, the topical application of Cam003 at 6 h following the infectious challenge was not sufficient to diminish the bacterial corneal burden and the accompanying inflammation (Fig. 3B and C). No changes in neutrophil influx were observed, as measured by corneal neutrophil elastase levels or by neutrophil attracting cytokines IL-1 β and MIP-2 (Fig. 3C).

3.3 | SW mice are resistant to *P. aeruginosa* keratitis

To identify modalities that may promote efficient bacterial clearance, we examined immune responses to *P. aeruginosa*-induced keratitis in SW and C57BL6/N mice. Unlike the C57BL6/N mice, the SW mice appeared resistant to infection and cleared *P. aeruginosa* (Fig. 4A). This correlated with the *ex vivo* ability of SW-derived neutrophils to kill *P. aeruginosa* more efficiently than the C57BL6/N-derived neutrophils (Fig. 4B).

To identify potential molecular mechanisms responsible for the improved bactericidal activity of SW-derived neutrophils, quantitative proteomic analysis was performed on neutrophils derived from noninfected (baseline) and *P. aeruginosa*-infected SW and C57BL6/N mice. In total, 4297 proteins were identified from triplicate samples of SW baseline, SW infected, C57BL6/N baseline, and C57BL6/N infected cells. Biologic replicate reproducibility ranged from 92% to 95%. A

PCA demonstrated clear clustering of the biologic replicates (Fig. 5A) and distinct patterns of protein responses among the strains and treatments (component 1 at 37.2%; component 2 at 16.3%), illustrating active remodeling of the proteomes in the neutrophils derived from the infected mice. The volcano plots compare the differentially present proteins across genotypes (SW versus C57BL6/N). We identified 366 proteins with significant differences in abundance upon comparison of PMN proteomes (Fig. 5B). Additionally, we identified 695 proteins with significant differences in abundance upon comparison of PMN proteomes derived from infected SW and C57BL6/N mice (Fig. 5C).

Interestingly, 1D annotation enrichment profiling based on keywords of the significantly different neutrophil proteins (*P* value < 0.05; FDR < 0.05) identified among the comparisons, revealed patterns of enrichment between the proteomes of neutrophils derived from infected C57BL6/N mice versus noninfected C57BL6/N mice (Fig. 5D comparison 1) and between the proteomes of neutrophils derived from the infected C57BL6/N and infected SW mice (Fig. 5D. comparison 4). These results suggest clear differences in neutrophil responses during infection in the C57BL6/N strain, as well as differential neutrophil outcomes between the mouse strains. Namely, neutrophil responses to infection included proteins associated with translocation, spliceosome formation, regulation of mRNA splicing, mRNA processing,

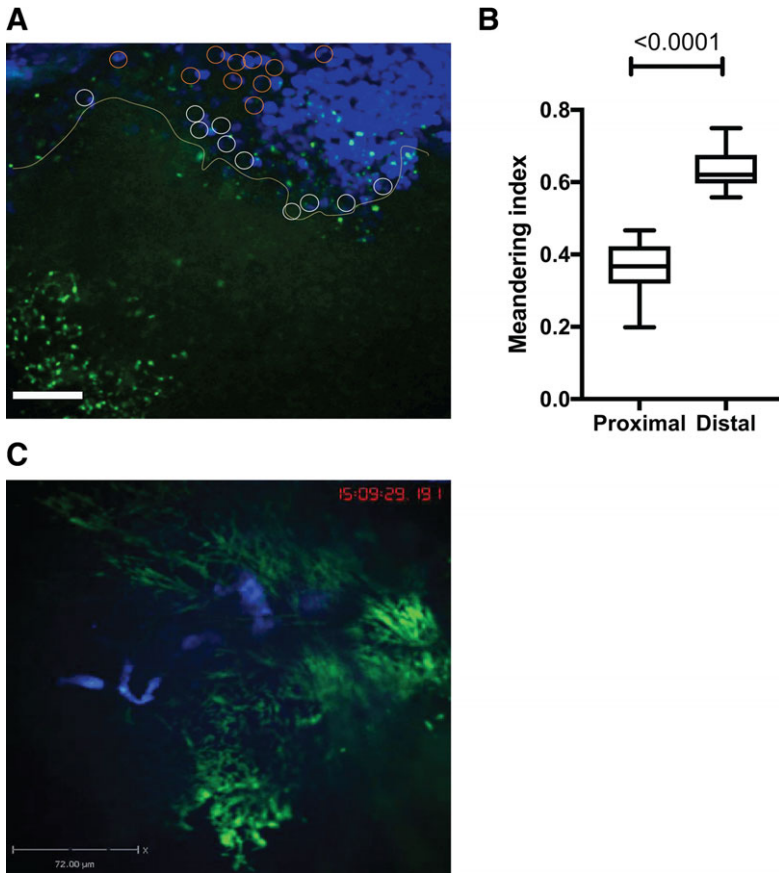


FIGURE 2 Neutrophils do not penetrate bacterial biofilms. C57BL6/N mouse was infected with 1×10^5 CFU/eye PAO1-GFP. Mice were given fluorescent anti-Ly6G-Alexa 647 IV to label neutrophils. (A) Neutrophil swarms were migrating towards bacterial biofilms (green). Still image from S1. Bar size $72 \mu\text{m}$. (B) Meandering indexes were calculated using MatLab and plotted. Neutrophil motilities differed depending on whether neutrophils appeared proximal to the biofilm (white circles) or distal (orange circles). Proximally located PMNs had significantly lower motilities when compared to the ones within the swamps or at a distance where bacteria were planktonic. Student's *t* test. S1 movie is representative of three independent experiments. (C) Crawling neutrophils (blue) probe the bacterial clusters (green) (Still image from S2). *P. aeruginosa* PAO1 appear green, less mobile, and individual bacterial cells visibly move back and forth demonstrating restricted mobility within microcolonies. The movie displays crawling neutrophils that probe bacterial microcolonies, but do not enter them. The movie is representative of more than three independent experiments. Video recording, 50 min

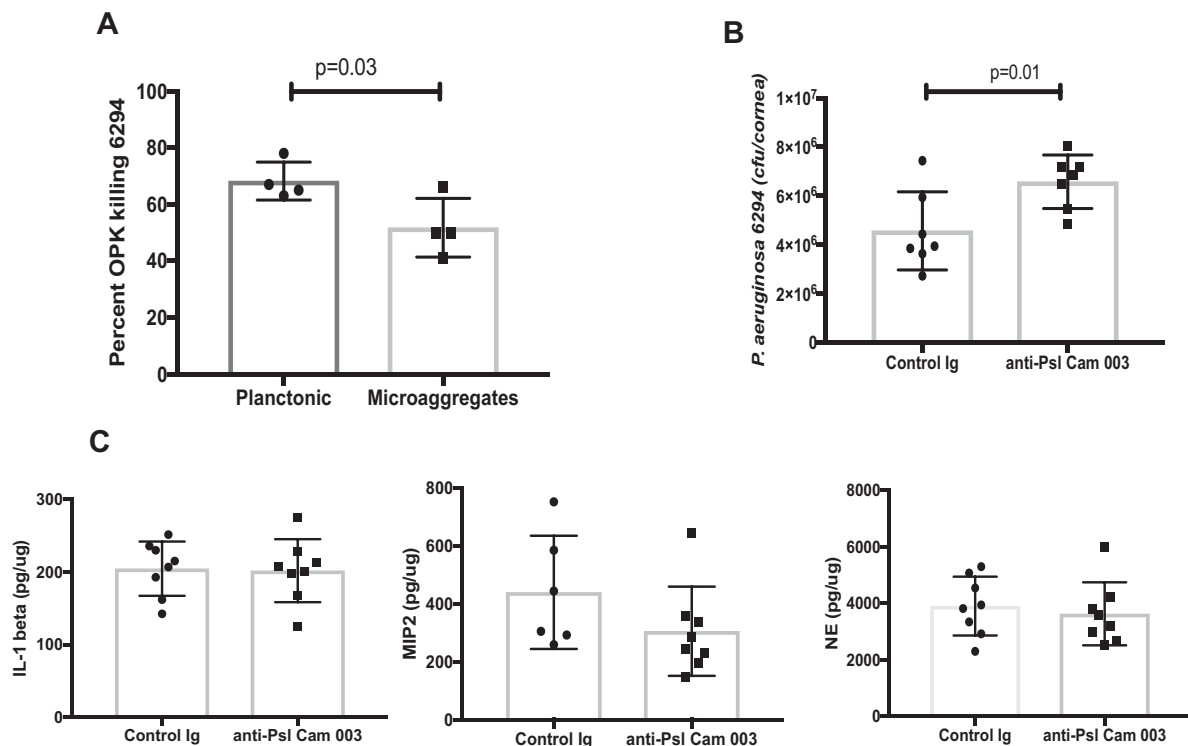


FIGURE 3 Topical application of anti-*psl* MAb Cam003 is not protective. (A) Percent OPK of *P. aeruginosa* 6294 grown in a planktonic and microaggregate form. The anti-*Psl* mAb Cam003 shows significant opsonophagocytic killing against 6294, which is decreased when bacteria are allowed to form microaggregates in vitro. Student's *t* test. (B) Topical application of $400 \mu\text{g}$ of Cam 003 onto infected eyes does not improve bacterial clearance. The mAb-treated eyes show a 2-fold increase in bacterial presence. Student's *t* test. $P = 0.01$. Data are representative of three independent experiments. (C) No significant differences in tissue IL- 1β , MIP-2, and NE levels among Cam 003-treated and control Ab-treated mice. Student's *t* test. Each symbol represents individual animals

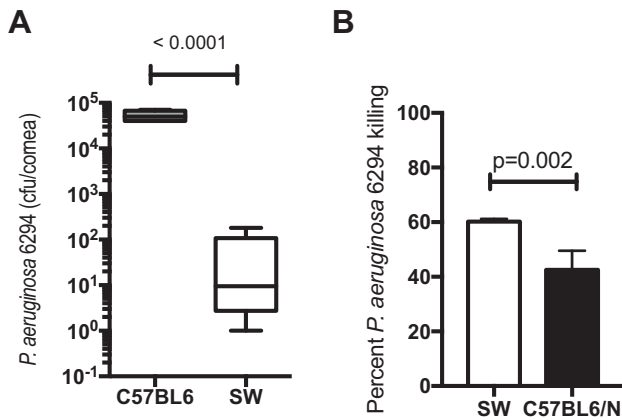


FIGURE 4 SW mice are resistant to *P. aeruginosa* 6294-induced keratitis. (A) Cohorts of SW ($N = 9$) and C57BL/6 ($N = 5$) mice were infected with 1×10^6 CFU of *P. aeruginosa* 6294 and bacterial burdens in the cornea quantified at 48 h after the onset of infection. Student's *t* test. Experiments were repeated thrice. (B) SW-derived PMNs kill *P. aeruginosa* 6294 more efficiently than C57BL/6N-derived PMNs. Mature neutrophils were purified from bone marrow of SW and C57BL/6N mice (stem cell), and exposed to 6294 at MOI 1 for 90 min as in Dwyer and Gadjeva, and Ray. Aliquots from the reactions were plated. Student's *t* test. Data are representative of two independent experiments

RNA-binding, and methylation. Positive enrichment of membrane-associated proteins was also observed including transmembrane proteins, transmembrane helix proteins, and mitochondrion inner membrane proteins, which suggests that processes of cellular remodeling are involved. Finally, secreted proteins and proteins of the endoplasmic reticulum were positively enriched, indicating secretory pathway involvement as a response to infection, which may be a potential connection with the observed α -mannosidase activity and secretion. Similarities in lower-limit enrichment was observed for enzymatic processes (e.g., ligase, serine/threonine-protein kinase, GTPase activation, and Ubl conjugation), cellular compartments (e.g., cytoplasm), and general cellular processes (e.g., ATP-binding), suggesting reduced involvement during infection. Conversely, strain-specific differences in neutrophil responses through positive enrichment showed differential responses of lectin and calcium-associated pathways, indicating changes in cellular processes and metabolism. Additionally, differences in lower-limit enrichment included differences in kinase, hydrolase, transferase, and nucleotide-binding categories, associated with post-translational modifications and cellular regulation.

Only two categories of proteins stood out when comparing the 1D annotation enrichment keyword profiling between infected SW versus baseline SW (Fig. 5D-2) and baseline C57BL/6N versus baseline SW (Fig. 5D-3) proteomes. These included responses associated with post-translational modifications by acetylation which are typically involved in cell signaling, thereby enabling differential cellular reactions to perturbations, suggestive of infection-associated and strain-specific responses (Fig. 5D). Conversely, chaperone-associated proteins were positively enriched in a strain-specific manner, indicating changes in protein folding and cellular stress response. Taken together, these results demonstrated clear differences in protein enrichment profiles

between baseline and infection, as well as strain-specific responses, which likely contributed to the overall observations of differential neutrophil killing abilities between the mice strains.

Specifically, the abundance of lysosomal proteins with enzymatic activities were of particular interest due to differential patterns of regulation in the SW-derived PMNs at baseline and during infection. Namely, chitotriosidase-1 (Chit1) showed a 5.9- and 5.3-fold increase in abundance at baseline and during infection, respectively, as compared to C57BL/6N-derived proteomes; cathepsin E (CtsE) showed a 4.0-fold increase in abundance at baseline and during infection, respectively, as compared to the proteomes from C57BL/6N-derived neutrophils. Lysosomal α -mannosidase (Man2b1) showed a 5.0- and 2.9-fold increase in abundance at baseline and during infection, respectively, as compared to C57BL/6N neutrophils (Fig. 5B and C). Also of interest was α -mannosidase (Man2c1) which showed a 5.4-fold increase in abundance in infected SW-derived neutrophils as compared to infected C57BL/6N-derived neutrophils, but was not significantly different at baseline (Fig. 5C). Cumulatively, these data suggested that SW-derived neutrophils are more capable of producing proteins with anti-inflammatory and antimicrobial activities than their C57BL/6N counterparts. Further, our data showed that infection altered neutrophil proteomes demonstrating that these cells were significantly more plastic than previously appreciated and suggestive that the changes fine-tuned neutrophil responses to pathogens.

3.4 | Neutrophil cell intrinsic characteristics govern their superior bactericidal capacity against *P. aeruginosa*

To examine whether the differential killing of *P. aeruginosa* had cell-intrinsic component, neutrophil progenitor cell lines were developed from the bone marrow of both SW or C57BL/6N mice and allowed to mature in vitro to neutrophils (Fig. 6A). To verify that cell-intrinsic characteristics are responsible for differential killing of *P. aeruginosa*, SW-derived and C57BL/6N-derived neutrophil cell lines were matured with GCSF and their bactericidal capacities examined. Electron microscopy-based analysis of matured cells demonstrated appearance of cells with typical multilobed nuclei, characteristic to PMNs (Fig. 6A). Similar to the data generated with primary neutrophils, the in vitro SW-derived neutrophils were better at killing *P. aeruginosa* when compared to C57BL/6N-derived neutrophils (Fig. 6B, one-way ANOVA) even when exposed to GCSF priming.

To verify that the bactericidal activity of SW-derived neutrophils was dependent on α -mannosidases, GCSF-primed SW neutrophil cell line or bone marrow-derived primary neutrophils were pre-treated with the α -mannosidase inhibitor swainsonine and challenged with *P. aeruginosa* (Fig. 6C and D). In either of the comparisons, the SW neutrophil bactericidal activities were significantly reduced by swainsonine treatment (Fig. 6C, $P = 0.007$, Student's *t* test and Fig. 6D, $P = 0.02$, Student's *t* test), confirming the contribution of α -mannosidase in *P. aeruginosa* killing. Cumulatively, these data suggest that α -mannosidase facilitates bactericidal function of neutrophils.

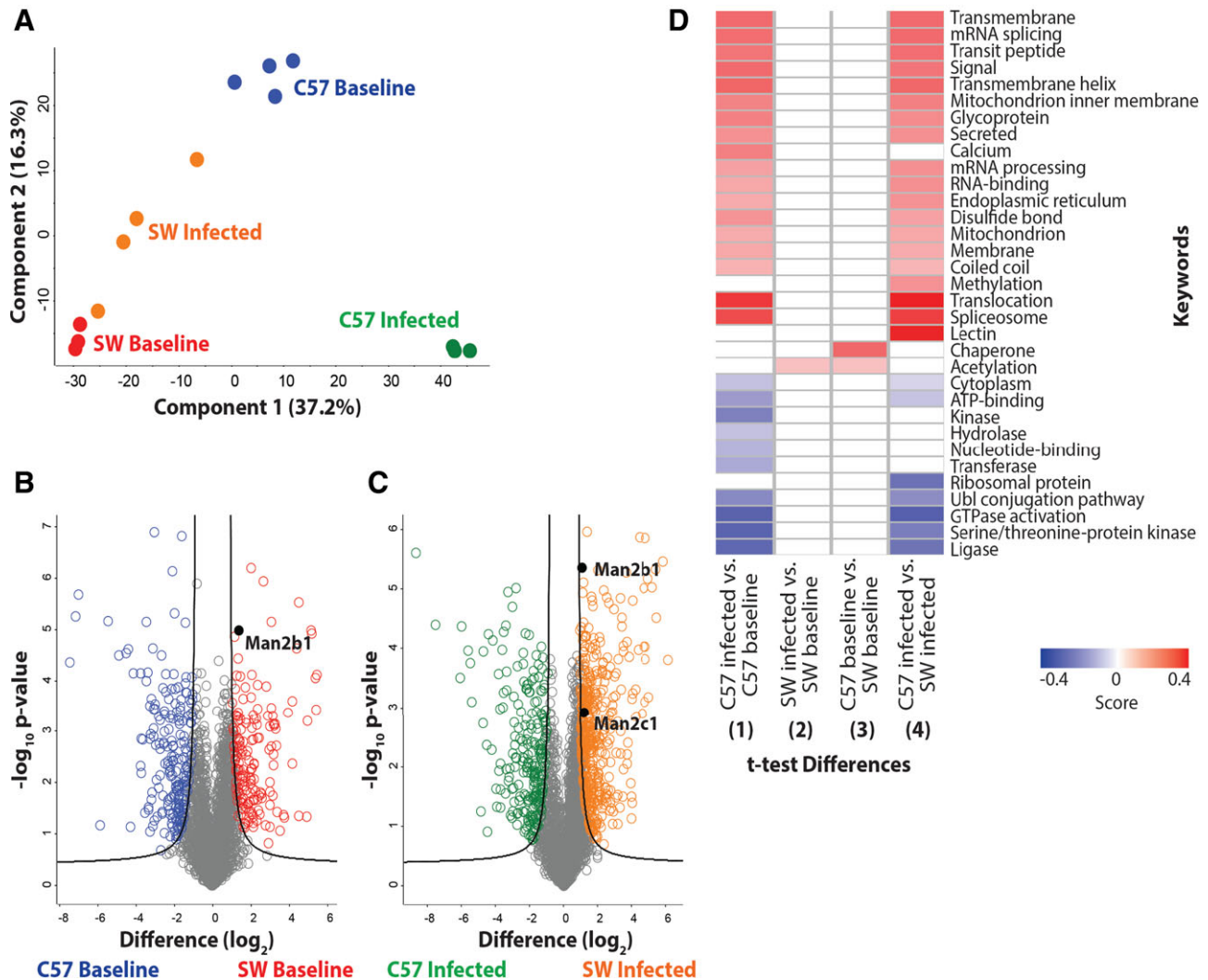


FIGURE 5 Differential protein abundance in SW and C57BL6/N-derived neutrophils from baseline and *P. aeruginosa*-infected mice. (A) Principle component analysis representing the proteomes of samples harvested from neutrophils derived from noninfected SW (red) and C57BL/6 mice (blue), and infected SW (orange) and C57BL/6 (green) mice. Experiment was performed with a minimum of biological triplicates and measured on the mass spectrometer in two independent experiments. (B) Volcano plot depicting all identified proteins in neutrophils harvested from noninfected SW and C57BL/6 mice. The significantly different proteins with an increase in abundance at baseline in SW mice are shown in red, whereas those in the C57BL6-derived neutrophils are shown in blue. Data are representative from two independent experiments performed in at least biological triplicate. A Welch's *t* test was performed to determine significant differences in protein abundance (P value < 0.05) using Benjamini-Hochberg FDR correction at 5%. The position of Man2b1 is highlighted. (C) Volcano plot depicting neutrophil proteomes from infected SW and C57BL/6 mice. The significantly different proteins with an increase in abundance during infection in SW mice are shown in orange, whereas those in the C57BL/6-derived neutrophils are shown in green. Data are representative from two independent experiments performed in at least biological triplicate. A Welch's *t* test was performed to determine significant differences in protein abundance (P value < 0.05) using Benjamini-Hochberg FDR correction at 5%. The position of Man2b1 and Man 2c1 are highlighted. (D) 1D annotation enrichment profile based on keywords for comparisons among baseline and infected SW and C57BL/6-derived neutrophil samples. Data are representative from two independent experiments performed in at least biological triplicate. A two-sample Student's *t* test was performed (P value < 0.05) using Benjamini-Hochberg FDR correction at 5% with scores between < -0.5 and < 0.5 .

3.5 | α -mannosidase treatment reduces bacterial burden during keratitis

Given that Psl is a mannose-rich polysaccharide and that α -mannosidase digests,³⁷ the biofilm-reducing capacity of exogenously added α -mannosidase was examined. Bacterial biofilms of *P. aeruginosa* 6294 were grown for 24 h and treated with α -mannosidase for 3 h at 37°C after biofilms had formed. Mannosidase treatment significantly reduced biofilm density (Fig. 7A, Student's *t* test, $P = 0.006$).

Further, a cyclic Di-GMP reporter PAO1 strain was allowed to form biofilms and was subsequently treated with α -mannosidase. The decrease in reporter-based fluorescence upon treatment accompanied the reduction in Psl-based biofilm formation (Fig. 7B, Student's *t* test, $P = 0.02$). Last, C57BL6/N mice were treated topically with α -mannosidase every 3 h for 12 h after the infectious challenge. Mice receiving topical mannosidase exhibited reduced bacterial burden when compared to the placebo-treated mice (Student's *t* test, $P = 0.008$) (Fig. 7C).

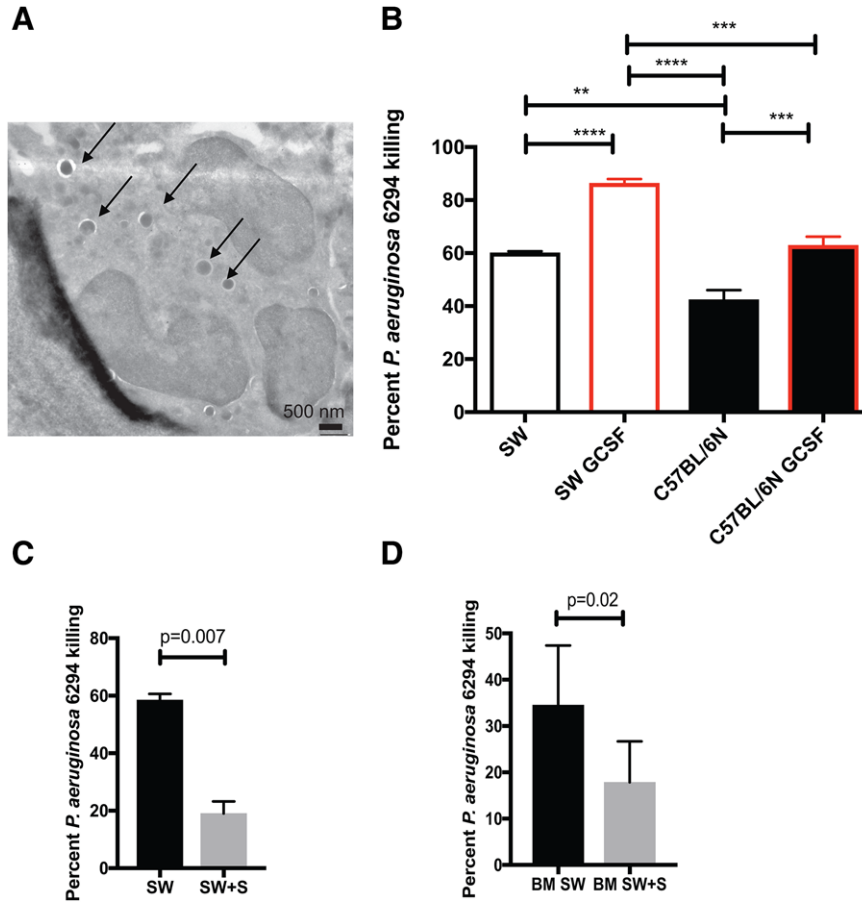


FIGURE 6 Swainsonine inhibits SW neutrophil bactericidal activities against *P. aeruginosa*. (A) Electron micrograph image of SW-cell line derived PMNs phagocytosing *P. aeruginosa*. Individual bacterial cells engulfed by the PMN are shown with arrows. (B) In vitro generated SW and C57BL/6N neutrophils were primed with GCSF and exposed to *P. aeruginosa*. Percent bacterial killing was calculated. One-way ANOVA. Data demonstrate that SW-derived neutrophils retain superior bactericidal activity over C57BL/6N neutrophils. Data are representative from one out of four individual experiments. (C) In vitro generated, primed with GCSF SW neutrophils were exposed swainsonine (SW+S) or vehicle control (SW) and challenged with *P. aeruginosa* 6294. Percent bacterial killing was calculated. Student's *t* test. Data are representative of two experiments. (D) Bone marrow-derived SW neutrophils were exposed to swainsonine and *P. aeruginosa*. Percent bacterial killing was calculated. Student's *t* test

4 | DISCUSSION

To date, the in-depth analysis of bacterial biofilms at ocular surfaces has been hindered by the lack of information about the nature of the bacterial polysaccharides in the matrix, lack of polysaccharide specific antibodies, imaging that requires tissue fixation and ex vivo analysis of corneas.²² Using intravital imaging in live animals, we demonstrated that ocular *P. aeruginosa* biofilms are Psl rich. Consequently, our data suggest a niche-specific adaptation of *P. aeruginosa*. Based on these observations we reason that treatment of ocular keratitis could be tailored to that niche.

Although the majority of keratitis isolates produce Psl,¹⁸ we cannot exclude contributions from other polysaccharides or matrix components in *P. aeruginosa* biofilms. For example, it is known that PA14 lacks Psl, is virulent in ocular keratitis models. Hence, it is likely that Psl is sufficient for *P. aeruginosa* pathoadaptation to the ocular niche, but not required.

Interestingly, the administration of the anti-Psl mAb was not sufficient to ameliorate keratitis, despite its excellent in vitro OPK characteristics. Indeed, we observed a 2-fold increase in the recovered bacteria from the infected corneas of the mAb-treated group (Fig. 3). A possible explanation is lack of penetrance of neutrophils inside the biofilm even when biofilm were covered with anti-Psl- specific antibodies. Fewer neutrophils were present at the surface or close to the surface of the biofilms, whereas the majority of the neutrophils appeared under the biofilms, within the epithelial and/or stromal layer

of the eye. Because Psl covered and surrounded bacterial biofilms at the ocular surface, the lack of therapeutic effect may be explained with the reduced neutrophil presence. Alternatively, defects in ability of neutrophils to digest biofilms even in the presence of polysaccharide-specific antibodies may contribute to the process, which would be consistent with the data presented here. Last, additional virulence factors may impair neutrophil functionality in the vicinity of biofilms. Given the recently reported benefit of the bispecific anti-Psl and anti-PcrV antibody in multiple animal infection models,^{8,38,39} it is likely that targeting of the type III secretion system is needed to confer protection.

To identify modalities that promote efficient bacterial clearance, we examined immune responses to *P. aeruginosa*-induced keratitis in SW and C57BL/6N mice. Unlike the C57BL/6N mice, the SW mice appeared resistant to infection and cleared *P. aeruginosa* in vivo. This correlated with the ability of SW-derived neutrophils to kill *P. aeruginosa* in vitro more efficiently than C57BL/6N-derived neutrophils.

To identify potential mechanisms for improved bactericidal activity, we used quantitative LC-MS approach. We identified more than 4000 total proteins per neutrophil proteome, which exceeds significantly the pool of 2000 proteins reported in previous proteomic studies.⁴⁰⁻⁴³ Based on our proteomic data, we identified infection and strain-specific differences in the neutrophil proteomic networks.

For the purposes of this particular investigation we chose to focus on α -mannosidases that were significantly more abundant in the neutrophils derived from the SW mice, suggestive of their contribution to protective immunity. Because Psl is a polymer of pentameric repeating

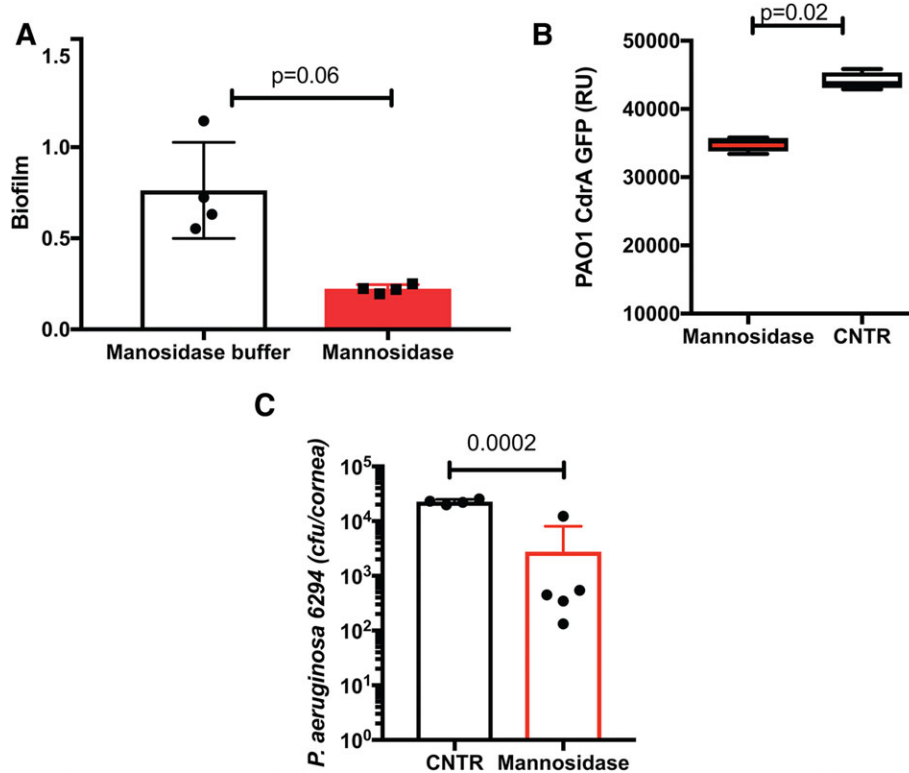


FIGURE 7 Alpha mannosidase treatment facilitates *P. aeruginosa* clearance in C57BL/6N mice. (A) *P. aeruginosa* 6294 was allowed to form biofilms in vitro for 24 h and were exposed to 10 U of α -mannosidase for 2 h at 37°C. Bacterial biofilms stained and measured. Student's *t* test. ($P = 0.006$). Data are representative of two experiments. (B) *P. aeruginosa* PAO1-CrdA-GFP was allowed to form biofilms in vitro for 24 h and were exposed to 10 U of α -mannosidase for 2 h at 37°C. Bacterial biofilms were washed, and fluorescent signal measured. Student's *t* test. ($P = 0.05$). Data are representative of two independent experiments. (C) C57BL/6N were infected with *P. aeruginosa* 6294 at 1.10^6 CFU/cornea, treated with 0.2 U/drop α -mannosidase four times daily, starting at 12 h post the onset of infection. Student's *t* test, ($P = 0.01$). Data are representative of two independent experiments with 5 mice per group

units of D-mannose, L-rhamnose, and D-glucose, where the individual α -D-mannose residues are connected with linkages, suitable for digest by the identified via LC-MS/MS α -mannosidases (e.g., Man2b1), we tested the importance of α -mannosidases in regulating biofilm formation and bactericidal properties of neutrophils. Consistent with recently published data by others,⁴⁴ we observed that treatment with α -mannosidase in vitro decreased *P. aeruginosa* biofilms. Another recent study demonstrated that α -mannosidase targeted Psl.³⁷ Furthermore, Psl inhibited neutrophil bactericidal activity³⁷ and protected bacteria from proteolytic attack by neutrophil elastase.²⁵ We confirmed and expanded on this foundation by providing evidence that neutrophil-derived α -mannosidase activity is needed for optimal bactericidal function against *P. aeruginosa* and that the topical application of α -mannosidase decreased corneal bacterial burden in vivo at least initially during infection (Fig. 7). Cumulatively, these findings suggested that exogenous α -mannosidases alter Psl structure in such a way that render *P. aeruginosa* more susceptible to killing.

In humans, α -mannosidase is present in the lysosomes and is secreted extracellularly^{45,46} Mutations that impair lysosomal α -mannosidase (Man2b1) activity cause development of α -mannosidosis, a condition that is rare, autosomal recessive, and multisystemic. This progressive lysosomal storage disorder results in facial and skeletal abnormalities, motor impairment, hearing impairment, intellectual disability, immune deficiency, and recurrent infections.⁴⁷ Importantly, the

recombinant human α -mannosidase shows promise in clinical trials for enzyme replacement therapy.⁴⁸ The recombinant α -mannosidase is well tolerated; the frequency of infusion-related reactions and the development of allo-antibodies are low compared to other enzyme replacement therapies.⁴⁸ These findings are exciting as they suggest that the use of recombinant human α -mannosidase for treatment of other conditions such as treatment of biofilm-based infections may be feasible and well tolerated.

The pool of differentially expressed proteins also included additional proteins such as cathepsin E (4.7-fold), CD14 (2.5-fold), and Chit1 (3.6-fold). Previous studies have documented that CD14 deficiency was associated with altered kinetics of *P. aeruginosa*-induced keratitis, implicating CD14-triggered pathways in promoting inflammation-induced corneal tissue damage in the C57BL/6 mice.⁴⁹ Consistently, Chit1 deficiency altered inflammatory responses to *K. pneumoniae* in the infected lungs of C57BL6 mice, resulting in less pathology.⁵⁰ Last, overexpression of cathepsin E was associated with alterations in the kinetics of phagolysosomal assembly, terminating phagolysosomal maturation.⁵¹ Cumulatively, these data illustrate that the infected SW-derived PMNs had proteomes that bear unique features, reflective of distinct neutrophil functions that were associated with improved recovery. It is of our current interest to find out how to leverage this knowledge therapeutically to promote resolution of infection.

AUTHORSHIP

A.K., R.M., E.G., and M.G. performed experiments and analyzed data. J.G.-M. generated and analyzed the LC-MS data. D.B.S. and M.K.M. provided insight and helped generating PMN cell lines. A.D.G. provided the anti-psl MoAb. M.G. conceptualized the study, analyzed data, and wrote the manuscript. All authors critically read the manuscript.

ACKNOWLEDGMENTS

This work was supported by NIH-NEI RO1 EY022054 to M.G. The authors thank Dr. Ajitha Thanabalasuriar and Prof. P. Kubes (University of Calgary, Canada) for providing expertise and help during the initial experiments of imaging of bacterial biofilms. They also thank Maria Ericsson (Harvard Electron Microscopy [EM] core) for EM analysis.

DISCLOSURES

A.D.G. has interests in developing anti-Psl-MoAb-based therapies.

REFERENCES

- Robertson DM, Petroll WM, Jester JV, Cavanagh HD. The role of contact lens type, oxygen transmission, and care-related solutions in mediating epithelial homeostasis and pseudomonas binding to corneal cells: an overview. *Eye Contact Lens*. 2007;33:394-398. discussion 399-400.
- Robertson DM, Petroll WM, Jester JV, Cavanagh HD. Current concepts: contact lens related Pseudomonas keratitis. *Cont Lens Anterior Eye*. 2007;30:94-107.
- Fleiszig SM, Evans DJ. The pathogenesis of bacterial keratitis: studies with Pseudomonas aeruginosa. *Clin Exp Optom*. 2002;85:271-278.
- Fleiszig SM, The Glenn A. Fry award lecture 2005. The pathogenesis of contact lens-related keratitis. *Optom Vis Sci*. 2006;83:866-873.
- O'Brien TP, Maguire MG, Fink NE, Alfonso E, McDonnell P. Efficacy of ofloxacin vs cefazolin and tobramycin in the therapy for bacterial keratitis. Report from the Bacterial Keratitis Study Research Group. *Arch Ophthalmol*. 1995;113:1257-1265.
- Andrews T, Sullivan KE. Infections in patients with inherited defects in phagocytic function. *Clin Microbiol Rev*. 2003;16:597-621.
- Vareechon C, Zmina SE, Karmakar M, Pearlman E, Rietsch A. Pseudomonas aeruginosa effector ExoS inhibits ROS production in human neutrophils. *Cell Host Microbe*. 2017;21:611-618. e5.
- Thanabalasuriar A, Surewaard BG, Willson ME, et al. Bispecific antibody targets multiple Pseudomonas aeruginosa evasion mechanisms in the lung vasculature. *J Clin Invest*. 2017;127:2249-2261.
- Lovewell RR, Patankar YR, Berwin B. Mechanisms of phagocytosis and host clearance of Pseudomonas aeruginosa. *Am J Physiol Lung Cell Mol Physiol*. 2014;306:L591-603.
- Fleiszig SM, Evans DJ, Do N, Vallas V, Shin S, Mostov KE. Epithelial cell polarity affects susceptibility to Pseudomonas aeruginosa invasion and cytotoxicity. *Infect Immun*. 1997;65:2861-2867.
- Fleiszig SM, Zaidi TS, Fletcher EL, Preston MJ, Pier GB. Pseudomonas aeruginosa invades corneal epithelial cells during experimental infection. *Infect Immun*. 1994;62:3485-3493.
- Fleiszig SM, Zaidi TS, Pier GB. Pseudomonas aeruginosa invasion of and multiplication within corneal epithelial cells in vitro. *Infect Immun*. 1995;63:4072-4077.
- Jennings LK, Storek KM, Ledvina HE, et al. Pel is a cationic exopolysaccharide that cross-links extracellular DNA in the Pseudomonas aeruginosa biofilm matrix. *Proc Natl Acad Sci U S A*. 2015;112:11353-11358.
- Parsek MR. Controlling the Connections of Cells to the Biofilm Matrix. *J Bacteriol*. 2016;198:12-14.
- Ma L, Lu H, Sprinkle A, Parsek MR, Wozniak DJ. Pseudomonas aeruginosa Psl is a galactose- and mannose-rich exopolysaccharide. *J Bacteriol*. 2007;189:8353-8356.
- Colvin KM, Irie Y, Tart CS, et al. The Pel and Psl polysaccharides provide Pseudomonas aeruginosa structural redundancy within the biofilm matrix. *Environ Microbiol*. 2012;14:1913-1928.
- Zhao K, Tseng BS, Beckerman B, et al. Psl trails guide exploration and microcolony formation in Pseudomonas aeruginosa biofilms. *Nature*. 2013;497:388-391.
- Zegans ME, DiGiandomenico A, Ray K, et al. Association of biofilm formation, Psl exopolysaccharide expression, and clinical outcomes in Pseudomonas aeruginosa keratitis: analysis of isolates in the steroids for corneal ulcers trial. *JAMA Ophthalmol*. 2016;134:383-389.
- Zaidi T, Pier GB. Prophylactic and therapeutic efficacy of a fully human immunoglobulin G1 monoclonal antibody to Pseudomonas aeruginosa alginate in murine keratitis infection. *Infect Immun*. 2008;76:4720-4725.
- Ma L, Conover M, Lu H, Parsek MR, Bayles K, Wozniak DJ. Assembly and development of the Pseudomonas aeruginosa biofilm matrix. *PLoS Pathogens*. 2009;5:e1000354.
- Ghafoor A, Hay ID, Rehm BH. Role of exopolysaccharides in Pseudomonas aeruginosa biofilm formation and architecture. *Appl Environ Microbiol*. 2011;77:5238-5246.
- Saraswathi P, Beuerman RW. Corneal biofilms: from planktonic to microcolony formation in an experimental keratitis infection with Pseudomonas aeruginosa. *Ocular Surf*. 2015;13:331-345.
- Kragh KN, Alhede M, Jensen PO, et al. Polymorphonuclear leukocytes restrict growth of Pseudomonas aeruginosa in the lungs of cystic fibrosis patients. *Infect Immun*. 2014;82:4477-4486.
- Mishra M, Byrd MS, Sergeant S, et al. Pseudomonas aeruginosa Psl polysaccharide reduces neutrophil phagocytosis and the oxidative response by limiting complement-mediated opsonization. *Cell Microbiol*. 2012;14:95-106.
- Tseng BS, Reichhardt C, Merrihew GE, et al. A biofilm matrix-associated protease inhibitor protects Pseudomonas aeruginosa from proteolytic attack. *MBio*. 2018;9.
- Rybtke MT, Borlee BR, Murakami K, et al. Fluorescence-based reporter for gauging cyclic di-GMP levels in Pseudomonas aeruginosa. *Appl Environ Microbiol*. 2012;78:5060-5069.
- Preston MJ, Fleiszig SM, Zaidi TS, et al. Rapid and sensitive method for evaluating Pseudomonas aeruginosa virulence factors during corneal infections in mice. *Infect Immun*. 1995;63:3497-3501.
- Dwyer M, Gadjeva M. Opsonophagocytic assay. *Methods Mol Biol*. 2014;1100:373-379.
- Odegaard JI, Vats D, Zhang L, et al. Quantitative expansion of ES cell-derived myeloid progenitors capable of differentiating into macrophages. *J Leukoc Biol*. 2007;81:711-719.
- DiGiandomenico A, Warriner P, Hamilton M, et al. Identification of broadly protective human antibodies to Pseudomonas aeruginosa exopolysaccharide Psl by phenotypic screening. *J Exp Med*. 2012;209:1273-1287.
- Kolaczowska E, Jenne CN, Surewaard BG, et al. Molecular mechanisms of NET formation and degradation revealed by intravital imaging in the liver vasculature. *Nat Commun*. 2015;6:6673.
- Rappsilber J, Mann M, Ishihama Y. Protocol for micro-purification, enrichment, pre-fractionation and storage of peptides for proteomics using StageTips. *Nat Protoc*. 2007;2:1896-1906.

33. Cox J, Mann M. MaxQuant enables high peptide identification rates, individualized p.p.b.-range mass accuracies and proteome-wide protein quantification. *Nat Biotechnol.* 2008;26:1367-1372.
34. Cox J, Neuhauser N, Michalski A, Scheltema RA, Olsen JV, Mann M. Andromeda: a peptide search engine integrated into the MaxQuant environment. *J Proteome Res.* 2011;10:1794-1805.
35. Cox J, Hein MY, Luber CA, Paron I, Nagaraj N, Mann M. Accurate proteome-wide label-free quantification by delayed normalization and maximal peptide ratio extraction, termed MaxLFQ. *Mol Cell Proteomics.* 2014;13:2513-2526.
36. Tyanova S, Temu T, Sinitcyn P, et al. The Perseus computational platform for comprehensive analysis of (prote)omics data. *Nat Methods.* 2016;13:731-740.
37. Hill PJ, Scordo JM, Arcos J, et al. Modifications of *Pseudomonas aeruginosa* cell envelope in the cystic fibrosis airway alters interactions with immune cells. *Sci Rep.* 2017;7:4761.
38. Le HN, Quetz JS, Tran VG, et al. MEDI3902 correlates of protection against severe *Pseudomonas aeruginosa* pneumonia in a rabbit acute pneumonia model. *Antimicrob Agents Chemother.* 2018:62.
39. DiGiandomenico A, Keller AE, Gao C, et al. A multifunctional bispecific antibody protects against *Pseudomonas aeruginosa*. *Sci Transl Med.* 2014;6:262ra155.
40. Loi ALT, Hoonhorst S, van Aalst C, et al. Proteomic profiling of peripheral blood neutrophils identifies two inflammatory phenotypes in stable COPD patients. *Respir Res.* 2017;18:100.
41. Tak T, Wijten P, Heeres M, et al. Human CD62L(dim) neutrophils identified as a separate subset by proteome profiling and in vivo pulse-chase labeling. *Blood.* 2017;129:3476-3485.
42. McLeish KR, Merchant ML, Klein JB, Ward RA. Technical note: proteomic approaches to fundamental questions about neutrophil biology. *J Leukoc Biol.* 2013;94:683-692.
43. Serwas NK, Huemer J, Dieckmann R, et al. CEBPE-mutant specific granule deficiency correlates with aberrant granule organization and substantial proteome alterations in neutrophils. *Front Immunol.* 2018;9:588.
44. Banar M, Emaneini M, Satarzadeh M, et al. Evaluation of mannosidase and trypsin enzymes effects on biofilm production of *Pseudomonas aeruginosa* isolated from burn wound infections. *PLoS one.* 2016;11:e0164622.
45. Rose DR. Structure, mechanism and inhibition of Golgi alpha-mannosidase II. *Current Opin Struct Biol.* 2012;22:558-562.
46. Tasegian A, Paciotti S, Ceccarini MR, et al. Origin of alpha-mannosidase activity in CSF. *Int J Biochem Cell Biol.* 2017;87:34-37.
47. Borgwardt L, Lund AM, Dali CI. Alpha-mannosidosis - a review of genetic, clinical findings and options of treatment. *Pediatr Endocrinol Rev.* 2014;12(Suppl 1):185-191.
48. Borgwardt L, Dali CI, Fogh J, et al. Enzyme replacement therapy for alpha-mannosidosis: 12 months follow-up of a single centre, randomised, multiple dose study. *J Inher Metabol Dis.* 2013;36:1015-1024.
49. Roy S, Karmakar M, Pearlman E. CD14 mediates toll-like receptor 4 (TLR4) endocytosis and spleen tyrosine kinase (Syk) and interferon regulatory transcription factor 3 (IRF3) activation in epithelial cells and impairs neutrophil infiltration and *Pseudomonas aeruginosa* killing in vivo. *J Biol Chem.* 2014;289:1174-1182.
50. Sharma L, Amick AK, Vasudevan S, et al. Regulation and role of chitotriosidase during lung infection with *Klebsiella pneumoniae*. *J Immunol.* 2018;201:615-626.
51. Tsukuba T, Yanagawa M, Kadowaki T, et al. Cathepsin E deficiency impairs autophagic proteolysis in macrophages. *PLoS one.* 2013;8:e82415.
52. Ray VA, Hill PJ, Stover CK, et al. Anti-Psl Targeting of *Pseudomonas aeruginosa* Biofilms for Neutrophil-Mediated Disruption. *Sci Rep.* 2017;7:16065.

SUPPORTING INFORMATION

Additional information may be found online in the Supporting Information section at the end of the article.

How to cite this article: Kugadas A, Geddes-McAlister J, Guy E, et al. Employing enzymatic treatment options for management of ocular biofilm-based infections. *J Leukoc Biol.* 2019;105:1099-1110. <https://doi.org/10.1002/JLB.4HI0918-364RR>